

Improved Efficient Two-Stage Denoising Diffusion Power System Measurement Recovery Against False Data Injection Attacks and Data Losses

Jianhua Pei, *Student Member, IEEE*, Jingyu Wang*, *Member, IEEE*, Dongyuan Shi, *Senior Member, IEEE*, and Ping Wang, *Fellow, IEEE*

Abstract—Measurement uncertainties, represented by cyber-attacks and data losses, seriously degrade the quality of power system measurements. Fortunately, the powerful generation ability of the denoising diffusion models can enable more precise measurement generation for power system data recovery. However, the controllable data generation and efficient computing methods of denoising diffusion models for deterministic trajectory still need further investigation. To this end, this paper proposes an improved two-stage denoising diffusion model (TSDM) to identify and reconstruct the measurements with various measurement uncertainties. The first stage of the model comprises a classifier-guided conditional anomaly detection component, while the second stage involves diffusion-based measurement imputation component. Moreover, the proposed TSDM adopts precise means and optimal variances to accelerate the diffusion generation process with subsequence sampling. Extensive numerical case studies demonstrate that the proposed TSDM can accurately recover power system measurements despite strong randomness under renewable energy integration and highly nonlinear dynamics under complex cyber-physical contingencies. Additionally, the proposed TSDM has stronger robustness compared to existing reconstruction networks and exhibits lower computational complexity than general denoising diffusion models.

Index Terms—Measurement uncertainty, state reconstruction, data recovery, denoising diffusion model, data loss.

I. INTRODUCTION

MODERN power systems typically exhibit a high level of complex nonlinear dynamics, high volatility, randomness, and intermittency due to the integration of renewable energy and the existence of interconnected cyber-physical power system events. In light of this, the new electric system has raised more concerns about the data quality issues of deployed remote terminal units (RTUs) in supervisory control and data acquisition (SCADA) and phasor measurement units (PMUs) in wide-area measurement systems (WAMS), as the accurately observed power system state variables reported by RTUs and PMUs often serve as input for many energy management applications [1]. However, measuring uncertainties, such as communication contingencies in extreme weather events and cyber-attacks in malicious threats, severely degrade the quality of power system measurements. Specifically, accidental network congestion or deliberate communication blocking can lead to data losses in the control center and manufactured data tampering attacks can cause the estimated system states to be biased, leading to the control center's incorrect decisions [2]. For this reason, adequate attention should be paid to investigating data recovery approaches against corrupted fragments in SCADA and WAMS.

The studies on power system measurement quality improvement can be mainly categorized into two groups. The first group is committed to solving the data quality problems caused by false data injection attack (FDIA) [3]. However, most of the studies on FDIA focus on how to launch attacks stealthily and

on defense mechanisms, and only a minority of the literature consider data recovery after suffering from FDIA. The generative adversarial network (GAN) model is employed to generate non-tampered data for recovering the compromised state variables [4]. A P-Q decomposition-based linear transformation approach is used to reconstruct contaminated state variables [5]. Nonetheless, the nonlinear nature of power flow may reduce the recovery accuracy. In [6], a state recovery approach is proposed based on the combination of quasi-Newton and Armijo line searches. However, successfully identifying the contaminated data by additional extreme learning machines is still necessary. The inertia of the power system is utilized for data restoration against FDIA with high accuracy and efficiency [7]. As the renewables-penetrated power systems may be low-inertia, the recovery error is high when state variables fluctuate dramatically.

The second category of studies makes great efforts to propose various complementation methods against data loss problems. The interpolation approaches, such as the Lagrangian interpolation and cubic spline interpolation [8], are widely used in power systems to synthesize missing data points or snippets. While this class of methods generally has fast speed, the interpolation performance may be seriously affected if outliers are contained in the measurements. Machine learning-based approaches using gated recurrent units (GRU) [9] and graph neural networks (GNN) [10] can achieve higher accuracy than interpolation approaches. However, this class of methods may have generalization issues when confronting unforeseen data distributions and complex nonlinearity in new-generation electric systems. To overcome the shortcoming of machine learning-based approaches, methods that utilize the low-rank property of PMU time-series are developed to recover missing data [11]–[13]. Among them, the alternating direction method of multiplier (ADMM) [14], [15] is utilized to improve the recovery accuracy and convergence speed when the measurements are accurately observed. Unfortunately, all these complementation approaches exhibit accuracy bottlenecks in the presence of measurement uncertainties.

The existing power system data recovery methods for FDIA and data loss issues still need improvement, such as improving recovery accuracy, expanding application scenarios, and reducing computational complexity. Compared with existing methods, denoising diffusion models, represented by the denoising diffusion probabilistic model (DDPM) [16] and the denoising diffusion implicit model (DDIM) [17], are better at generating realistic measurements with strong randomness and support

potential guided conditional data generation, making them more suitable for data recovery than existing generative models in practical power systems. In this paper, a two-stage denoising diffusion recovery model (TSDM) based on improved DDIMs is proposed to recover power system measurements under FDIA and data loss. The overall contribution of this approach is threefold:

- 1) A novel two-stage architecture is proposed, where the first stage uses a classifier-guided conditional diffusion component to detect and rectify outliers, and the second stage uses a measurement imputation diffusion component to synthesize missing data points or snippets.
- 2) Both stages are based on an enhanced DDIM model with low-length subsequences, which adopts the Bayesian theorem to estimate the precise mean and optimal variance to accelerate the data generation process.
- 3) The proposed TSDM demonstrates superiority in recovering SCADA measurements of power systems with renewable energy integration and WAMS measurements with highly nonlinear dynamics under complex power system contingencies .

The rest of this paper is organized as follows. Problem statement is presented in Section II. Section III briefly introduces the denoising diffusion models and classifier guidance. Section IV elaborates on the design of the proposed TSDM. Two aspects of performance demonstrations are given in Section V. Section VI concludes the paper. Supporting lemmas are included in the Appendix for reference.

II. PROBLEM STATEMENT

A. False Data Injection Attacks

Power systems usually operate in a quasi-steady state with slow and smooth changes in load or renewable energy generation. However, they transit to a transient state when faced with abrupt contingencies [18]. Generally, the SCADA system can effectively monitor the slow oscillations in the quasi-steady state. In contrast, the power system in the transient state requires the utilization of PMUs with higher reporting rates to record dynamic processes. To precisely describe and capture these steady and transient states, the generalized time discretization space model of the power system can be represented as

$$\mathbf{s}_k = f(\mathbf{s}_{k-1}, \mathbf{b}_{k-1}, \mathbf{u}_k, \mathbf{p}) + \mathbf{w}_k \quad (1)$$

$$\mathbf{z}_k = h(\mathbf{s}_k, \mathbf{u}_k, \mathbf{p}) + \mathbf{v}_k, \quad (2)$$

where \mathbf{s}_{k-1} and $\mathbf{s}_k \in \mathbb{R}^S$ are the power system state vectors at discrete timesteps $k-1$ and k , $\mathbf{z}_k \in \mathbb{R}^M$ is the measurement vector containing SCADA and PMU measurements, \mathbf{b}_{k-1} is the algebraic state vector, \mathbf{u}_k is the system control vector, \mathbf{p} is the model parameter, $f(\cdot)$ and $h(\cdot)$ are nonlinear functions, and \mathbf{w}_k and \mathbf{v}_k are the state and measurement errors subject to Normal distribution of zero mean and variance matrices of \mathbf{Q}_k and \mathbf{R}_k , respectively. Eq. (1) is the state-transition equation and Eq. (2) is the nonlinear observation equation.

The observation equation is usually utilized to finish the bad data detection (BDD) tasks in static state estimation (SSE) and dynamic state estimation (DSE) by computing the residual vector $\mathbf{r}_k = \mathbf{z}_k - h(\mathbf{s}_k)$. The elements in \mathbf{r}_k indicate whether

there are outliers in the corresponding measurements. For this reason, hackers covertly inject a false data component $\Delta \mathbf{z}_k^a$ into the measurement vector \mathbf{z}_k to offset the state vector \mathbf{s}_k with small enough \mathbf{r}_k^a . Regardless of the control vector and parameter changes, the tampered residual vector can be rewritten as

$$\mathbf{r}_k^a = \Delta \mathbf{z}_k^a - [h(\mathbf{s}_k + \Delta \mathbf{s}_k^a) - h(\mathbf{s}_k)]. \quad (3)$$

Evidently, the false data component $\Delta \mathbf{z}_k^a$ should be designed to minimize the residual vector \mathbf{r}_k^a . In this way, attackers can construct false data \mathbf{z}_k^a based on state vector offset $\Delta \mathbf{s}_k^a$. The general AC nonlinear FDIA model of SCADA and PMU data with incomplete network information can be described as

$$\begin{aligned} \text{obj : minimize } & \underbrace{\|\Delta(\mathbf{z}_k^a)^{\bar{\cup}} - [h^{\bar{\cup}}((\mathbf{s}_k^a)^{\bar{\cup}}) - h^{\bar{\cup}}(\mathbf{s}_k^{\bar{\cup}})]\|_0}_{(\mathbf{r}_k^a)^{\bar{\cup}}} \\ \text{s.t. : } & (\mathbf{s}_k^a)^{\bar{\cup}} = f^{\bar{\cup}}((\mathbf{s}_{k-1}^a)^{\bar{\cup}}) + \mathbf{w}_k^{\bar{\cup}}, |\theta_i^a - \theta_j^a| \leq |\theta_i - \theta_j|_{\max} \\ & \mathbf{s}_{\min}^{\bar{\cup}} \leq (\mathbf{s}_k^a)^{\bar{\cup}} \leq \mathbf{s}_{\max}^{\bar{\cup}}, |\delta_{Gi}^a - \delta_{Gj}^a| \leq |\delta_{Gi} - \delta_{Gj}|_{\max} \\ & P_{Gi}^{\min} \leq P_{Gi}^a \leq P_{Gi}^{\max}, Q_{Gi}^{\min} \leq Q_{Gi}^a \leq Q_{Gi}^{\max}, \end{aligned} \quad (4)$$

where $\bar{\cup}$ represents the power system area under cyber attacks, θ_i and θ_j are the voltage phase angles of Buses i and j , δ_{Gi} and δ_{Gj} are the power angles of Generators i and j , and P_{Gi} and Q_{Gi} are the active and reactive power output of Generator i . Through the above false data construction method and physical constraints, hackers only need to master incomplete power grid information $h^{\bar{\cup}}(\cdot)$ and $f^{\bar{\cup}}(\cdot)$ to inject false data that will not be recognized by BDD. In addition, from the time-series perspective, this paper assumes that hackers can launch six temporal forms of FDIA, i.e., step, ramp, random noises, replay, phase shift, and amplitude scaling attacks.

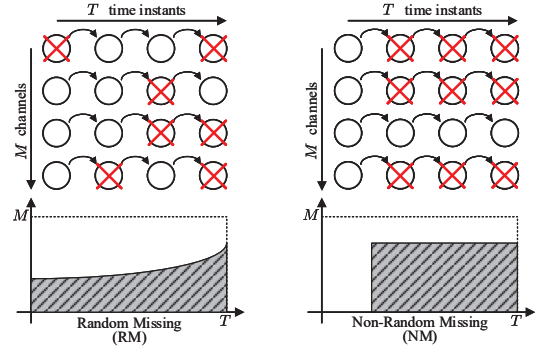


Fig. 1. Random and non-random data losses distribution of received measurements in power systems.

B. Data Losses

Power system measurements may be continuously missing due to communication malfunction, resulting in multi-channel non-random data losses. Moreover, random missing entries occur frequently as traditional bad data suppression and transmission delay exist in power systems. Anomaly detection in cyber power systems can result in data losses after removing contaminated data caused by data manipulation attacks. Unfortunately, when a large number of interlocking complex cyber attacks or communication malfunctions occur, the power system may become unobservable and uncontrollable. Collectively, this paper considers two forms of data loss,

i.e., random missing (RM) and non-random missing (NM) data. As depicted in Fig. 1, the received raw SCADA and PMU data consist of measurements from M measurement channels at T time instants.

According to the latency characteristics power system communication, the proportion of RM data is gamma distributed over time [19], and missing entries are randomly distributed in various measurement channels. On the contrary, the distribution of NM data is more regular, and NM usually results in sequential data loss at specific measurement channels.

III. DENOISING DIFFUSION MODELS

A. Denoising Diffusion Probabilistic Models

Denoising diffusion models are a class of machine learning algorithms inspired by Non-Equilibrium Thermodynamics that have better performance than generative models such as GANs. Diffusion models generally include a forward diffusion process and a reverse prediction process. The forward process of DDPM refers to gradually adding Gaussian noises to the original measurements $\mathbf{x}_0 \sim q(\mathbf{x}_0)$ until the measurements become random noises $\mathbf{x}_N \sim q(\mathbf{x}_N|\mathbf{x}_0)$ normally distributed with zero mean and unit variance, where $\mathbf{x}_0, \mathbf{x}_N \in \mathbb{R}^{M \times T}$ and $q(\cdot)$ is the distribution symbol. The forward process with N steps can be described as

$$q(\mathbf{x}_{1:N}|\mathbf{x}_0) = \prod_{n=1}^N q(\mathbf{x}_n|\mathbf{x}_{n-1}) \quad (5)$$

$$q(\mathbf{x}_n|\mathbf{x}_{n-1}) = \mathcal{N}(\sqrt{1 - \beta_n}\mathbf{x}_{n-1}, \beta_n \mathbf{I}),$$

where $\{\beta_n\}_{n=1}^N$ is the variance used for each step and $\beta_n \in (0, 1)$, and the variance schedule satisfies the relationship $\beta_1 < \beta_2 < \dots < \beta_N$. The forward process is a Markov chain, and \mathbf{x}_n at any step can be computed as

$$q(\mathbf{x}_n|\mathbf{x}_0) = \mathcal{N}(\sqrt{\alpha_n}\mathbf{x}_0, (1 - \alpha_n)\mathbf{I}), \quad (6)$$

where $\alpha_n = \prod_{i=1}^n (1 - \beta_i)$. As the number of diffusion steps increases, the signal ratio $\sqrt{\alpha_n}$ will gradually approach 0, while the noise ratio $\sqrt{1 - \alpha_n}$ will approach 1, ensuring that the final \mathbf{x}_N is close to a random noise $\epsilon \sim \mathcal{N}(0, \mathbf{I})$.

The reverse process of DDPM is opposite to the forward process in terms of noise elimination, i.e., the reverse process generates \mathbf{x}_0 from the random noise \mathbf{x}_N . In order to estimate the distribution $q(\mathbf{x}_{n-1}|\mathbf{x}_n)$, DDPM also defines the reverse process as a Markov chain and utilizes the neural network parameterized function $p_\theta(\mathbf{x}_{n-1}|\mathbf{x}_n) = \mathcal{N}(\mu_\theta(\mathbf{x}_n, n), \Sigma_\theta(\mathbf{x}_n, n))$ to predict the mean μ_θ and variance Σ_θ from \mathbf{x}_n at step n of the reverse process. DDPM ultimately obtains the training objective $L_{simple} = \mathbb{E}_{\mathbf{x}_0, \epsilon \sim \mathcal{N}(0, \mathbf{I})} [\|\epsilon - \epsilon_\theta(\mathbf{x}_n, n)\|^2]$ by considering the variational lower bound, where ϵ_θ is a neural network intended to predict the actual noise ϵ from \mathbf{x}_n .

B. Denoising Diffusion Implicit Models

Building upon DDPM, DDIM optimizes and accelerates the diffusion models by considering a non-Markov chain derivation. Since DDIM does not define a forward process, the target distribution of the reverse process

$$q(\mathbf{x}_{n-1}|\mathbf{x}_n, \mathbf{x}_0) = \frac{q(\mathbf{x}_n|\mathbf{x}_{n-1})q(\mathbf{x}_{n-1}|\mathbf{x}_0)}{q(\mathbf{x}_n|\mathbf{x}_0)} \quad (7)$$

should be obtained, considering that $q(\mathbf{x}_n|\mathbf{x}_{n-1})$ is not given. As a consequence, the derivation of the reverse process only needs to meet the marginal distribution condition. It can be inferred in [17] that the target distribution with variable standard deviation parameter σ_n for all $n \geq 2$ is

$$q_{\sigma_n}(\mathbf{x}_{n-1}|\mathbf{x}_n, \mathbf{x}_0) = \mathcal{N}(\sqrt{\alpha_{n-1}}\mathbf{x}_0 + \sqrt{1 - \alpha_{n-1} - \sigma_n^2} \frac{\mathbf{x}_n - \sqrt{\alpha_n}\mathbf{x}_0}{\sqrt{1 - \alpha_n}}, \sigma_n^2 \mathbf{I}). \quad (8)$$

Since \mathbf{x}_0 is unknown, the estimation $\bar{\mu}(\mathbf{x}_n)$ of \mathbf{x}_0 can be derived from $\mathbf{x}_n = \sqrt{\alpha_n}\mathbf{x}_0 + \sqrt{1 - \alpha_n}\epsilon$ as

$$\bar{\mu}(\mathbf{x}_n) = \frac{1}{\sqrt{\alpha_n}} [\mathbf{x}_n - \sqrt{1 - \alpha_n}\epsilon_\theta(\mathbf{x}_n, n)]. \quad (9)$$

Accordingly, during the generation phase, \mathbf{x}_{n-1} can be computed by the distribution q_{σ_n} , where the variable σ_n does not have any constraints. When $\sigma_n = \sqrt{(1 - \alpha_{n-1})/(1 - \alpha_n)}\sqrt{1 - \alpha_n/\alpha_{n-1}}$, the diffusion model becomes DDPM. When $\sigma_n = 0$, the reverse process of the diffusion model is deterministic, and the input random noise will generate fixed target measurements: this type of diffusion model is called DDIM.

C. Classifier Guidance

Diffusion models can be controlled to output the generation results according to the input condition \mathbf{y} , i.e., under the control of the measurement matrix $\mathbf{y}_0 \in \mathbb{R}^{M \times T}$ that consists of contaminated z_t^a over T time intervals. In this way, the diffusion models can generate corresponding restored power system measurements. In the reverse process, the most critical step is the construction of distribution $p_\theta(\mathbf{x}_{n-1}|\mathbf{x}_n)$. When the condition \mathbf{y} is added into the input, according to Bayes's theorem, the conditioned p_θ can be described as

$$p_\theta(\mathbf{x}_{n-1}|\mathbf{x}_n, \mathbf{y}) = \frac{p_\theta(\mathbf{x}_{n-1}|\mathbf{x}_n)p_\theta(\mathbf{y}|\mathbf{x}_{n-1}, \mathbf{x}_n)}{p_\theta(\mathbf{y}|\mathbf{x}_n)} \quad (10)$$

$$\approx p_\theta(\mathbf{x}_{n-1}|\mathbf{x}_n)e^{\log p_\theta(\mathbf{y}|\mathbf{x}_{n-1}) - \log p_\theta(\mathbf{y}|\mathbf{x}_n)}.$$

After Taylor expansion, the exponential term in Eq. (10) becomes

$$\log [p_\theta(\mathbf{y}|\mathbf{x}_{n-1})/p_\theta(\mathbf{y}|\mathbf{x}_n)] \approx (\mathbf{x}_{n-1} - \mathbf{x}_n) \nabla_{\mathbf{x}_n} \log p_\theta(\mathbf{y}|\mathbf{x}_n). \quad (11)$$

Consequently, the conditioned diffusion models with classifier guidance can approximately utilize the gradient $\nabla_{\mathbf{x}_n} \log p_\theta(\mathbf{y}|\mathbf{x}_n)$ to guide the random noises to gradually approach the target distribution. The gradient of the reverse process is $\nabla_{\mathbf{x}_n} \log p_\theta(\mathbf{x}_n|\mathbf{y})$, which can be transformed into $\nabla_{\mathbf{x}_n} \log p_\theta(\mathbf{x}_n) + \nabla_{\mathbf{x}_n} \log p_\theta(\mathbf{y}|\mathbf{x}_n)$ by Bayes's theorem. It can be seen from the score matching method that when the diffusion models predict noise ϵ_θ , $\nabla_{\mathbf{x}_n} \log p_\theta(\mathbf{x}_n)$ equals $-\epsilon_\theta(\mathbf{x}_n, n)/\sqrt{1 - \alpha_n}$, so the gradient can be rewritten as

$$\nabla_{\mathbf{x}_n} \log p_\theta(\mathbf{x}_n|\mathbf{y}) = -\frac{\epsilon_\theta(\mathbf{x}_n, n) - \sqrt{1 - \alpha_n} \nabla_{\mathbf{x}_n} \log p_\theta(\mathbf{y}|\mathbf{x}_n)}{\sqrt{1 - \alpha_n}}. \quad (12)$$

As a result, regardless of the variance of the generation process, the diffusion models only need to replace $\epsilon_\theta(\mathbf{x}_n, n)$ with $\epsilon_\theta(\mathbf{x}_n, n) - \sqrt{1 - \alpha_n} \nabla_{\mathbf{x}_n} \log p_\theta(\mathbf{y}|\mathbf{x}_n)$ to conditionally control the measurements generation process.

IV. IMPROVED EFFICIENT DIFFUSION RECOVERY METHOD

A. Optimal Variance

The traditional DDIM sets variance $\sigma_n = 0$ by default, and the generation process of diffusion model becomes a deterministic process. In order to accelerate the reverse process of DDIM, the data generation trajectory should be further optimized. Accordingly, the setting of optimal variance is considered as one of the means to accelerate the diffusion model. The target distribution in the reverse process of DDIM can be rewritten as

$$p(\mathbf{x}_{n-1}|\mathbf{x}_n, \mathbf{x}_0) = \mathcal{N}\left(\frac{\sqrt{1-\alpha_{n-1}-\sigma_n^2}}{\sqrt{1-\alpha_n}}\mathbf{x}_n + \underbrace{\left(\sqrt{\alpha_{n-1}} - \frac{\sqrt{1-\alpha_{n-1}-\sigma_n^2}\sqrt{\alpha_n}}{\sqrt{1-\alpha_n}}\right)}_{\gamma_n}\mathbf{x}_0, \sigma_n^2\mathbf{I}\right). \quad (13)$$

In classical DDIM, $\bar{\mu}(\mathbf{x}_n)$ estimated by \mathbf{x}_n is utilized to replace \mathbf{x}_0 in Eq. (13). Nevertheless, $\bar{\mu}(\mathbf{x}_n)$ predicted by \mathbf{x}_n can hardly be completely accurate, and the trajectory is uncertain. Consequently, the proposed improved diffusion model utilizes Normal distribution $\mathcal{N}(\bar{\mu}(\mathbf{x}_n), \bar{\sigma}_n^2\mathbf{I})$ with mean $\bar{\mu}(\mathbf{x}_n)$ and optimal variance $\bar{\sigma}_n^2$ to approximate \mathbf{x}_0 , and Eq. (13) can be transformed into a sampling form

$$\begin{aligned} \mathbf{x}_{n-1} &\approx \frac{\sqrt{1-\alpha_{n-1}-\sigma_n^2}}{\sqrt{1-\alpha_n}}\mathbf{x}_n + \gamma_n(\bar{\mu}(\mathbf{x}_n) + \bar{\sigma}_n\epsilon_2) + \sigma_n\epsilon_1 \\ &= \frac{\sqrt{1-\alpha_{n-1}-\sigma_n^2}}{\sqrt{1-\alpha_n}}\mathbf{x}_n + \gamma_n\bar{\mu}(\mathbf{x}_n) + \underbrace{(\sigma_n\epsilon_1 + \gamma_n\bar{\sigma}_n\epsilon_2)}_{\sim\sqrt{\sigma_n^2+\gamma_n^2\bar{\sigma}_n^2}\epsilon} \end{aligned} \quad (14)$$

where $\epsilon, \epsilon_1, \epsilon_2$ are i.i.d. as $\mathcal{N}(0, \mathbf{I})$. Evidently, $p(\mathbf{x}_{n-1}|\mathbf{x}_n)$ is closer to the Normal distribution with mean $\frac{\sqrt{1-\alpha_{n-1}-\sigma_n^2}}{\sqrt{1-\alpha_n}}\mathbf{x}_n + \gamma_n\bar{\mu}(\mathbf{x}_n)$ and covariance $(\sigma_n^2 + \gamma_n^2\bar{\sigma}_n^2)\mathbf{I}$, and even if $\sigma_n = 0$, the estimated variance of the reverse process is not zero. In summary, it is significant to estimate the optimal variance $(\gamma_n^2\bar{\sigma}_n^2)\mathbf{I}$. According to Eq. (9), the covariance of \mathbf{x}_n can be represented as

$$\begin{aligned} \Sigma(\mathbf{x}_n) &= \mathbb{E}_{\mathbf{x}_0 \sim p(\mathbf{x}_0|\mathbf{x}_n)} [(\mathbf{x}_0 - \bar{\mu}(\mathbf{x}_n))(\mathbf{x}_0 - \bar{\mu}(\mathbf{x}_n))^\top] \\ &= \frac{1}{\alpha_n} \underbrace{\mathbb{E}_{\mathbf{x}_0 \sim p(\mathbf{x}_0|\mathbf{x}_n)} [(\mathbf{x}_0 - \sqrt{\alpha_n}\mathbf{x}_0)(\mathbf{x}_0 - \sqrt{\alpha_n}\mathbf{x}_0)^\top]}_{\mathbf{e}_n} \\ &\quad - \frac{1-\alpha_n}{\alpha_n} \epsilon_\theta(\mathbf{x}_n, n)\epsilon_\theta(\mathbf{x}_n, n)^\top. \end{aligned} \quad (15)$$

According to the derivation of DDIM, it can be inferred that $p(\mathbf{x}_n|\mathbf{x}_0) = \mathcal{N}(\mathbf{x}_n; \sqrt{\alpha_n}\mathbf{x}_0, (1-\alpha_n)\mathbf{I})$ and the calculation result of \mathbf{e}_n can be represented as $(1-\alpha_n)\mathbf{I}$. Collectively, Eq. (15) can be rewritten as

$$\begin{aligned} \Sigma_n &= \mathbb{E}_{\mathbf{x}_n \sim p(\mathbf{x}_n)} [\Sigma(\mathbf{x}_n)] \\ &= \frac{1-\alpha_n}{\alpha_n} \left\{ \mathbf{I} - \mathbb{E}_{\mathbf{x}_n \sim p(\mathbf{x}_n)} [\epsilon_\theta(\mathbf{x}_n, n)\epsilon_\theta(\mathbf{x}_n, n)^\top] \right\}. \end{aligned} \quad (16)$$

Ultimately, both sides of Eq. (16) are traced and divided by the dimensionality d ($M \times T$) of power system measurements, then the optimal variance can be expressed as

$$\bar{\sigma}_n^2 = \frac{1-\alpha_n}{\alpha_n} \left\{ 1 - \frac{1}{d} \mathbb{E}_{\mathbf{x}_n \sim p(\mathbf{x}_n)} [\|\epsilon_\theta(\mathbf{x}_n, n)\|_2^2] \right\}. \quad (17)$$

B. Subsequence Acceleration

Compared with DDPM, DDIM does not clearly define the forward process in derivation, so DDIM can assume a forward process with shorter steps, i.e., DDIM can sample a subsequence $\tau = [\tau_1, \tau_2, \dots, \tau_s]$ with a length of s from the original sequence $[1, 2, \dots, N]$. Apparently, DDIM can reuse the diffusion model trained by DDPM, and the training results of DDPM essentially include the training results of its arbitrary subsequence parameter τ . As a result, DDIM can reduce the generation step size from N to s , and its computational complexity for power system data recovery will be reduced by s/N of the original. The diffusion model accelerated by subsequence is depicted in Fig. 2.

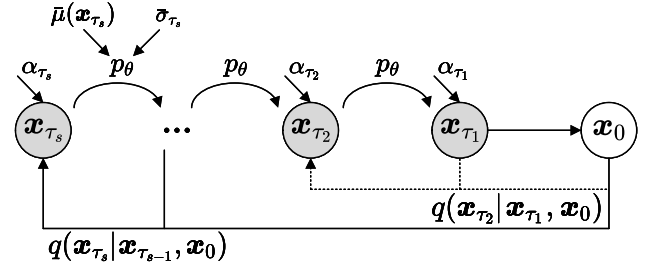


Fig. 2. Improved denoising diffusion implicit model with subsequence acceleration and parameterized reverse process p_θ .

Each step of the reverse process can be represented by the target distribution p_θ parameterized by the neural network, provided that the estimation $\bar{\mu}(\mathbf{x}_{\tau_i})$ of \mathbf{x} and optimal variance $\bar{\sigma}_{\tau_i}^2$ need to be calculated previously. Moreover, let

$$\Gamma_{\tau_i} = \sqrt{\alpha_{\tau_{i-1}}} - \frac{\sqrt{1-\alpha_{\tau_{i-1}}}\sqrt{\alpha_{\tau_i}}}{\sqrt{1-\alpha_{\tau_i}}}. \quad (18)$$

Conclusively, the final update equation with subsequence acceleration can be represented as

$$\mathbf{x}_{\tau_{i-1}} = \frac{\sqrt{1-\alpha_{\tau_{i-1}}}}{\sqrt{1-\alpha_{\tau_i}}}\mathbf{x}_{\tau_i} + \Gamma_{\tau_i}\bar{\mu}(\mathbf{x}_{\tau_i}) + \Gamma_{\tau_i}\bar{\sigma}_{\tau_i}\epsilon. \quad (19)$$

Alternatively, the detailed sampling form of p_θ can be described as

$$\begin{aligned} \mathbf{x}_{\tau_{i-1}} &= \frac{\sqrt{\alpha_{\tau_{i-1}}}}{\sqrt{\alpha_{\tau_i}}}\mathbf{x}_{\tau_i} + \left(\sqrt{\alpha_{\tau_{i-1}}} - \frac{\sqrt{1-\alpha_{\tau_{i-1}}}\sqrt{\alpha_{\tau_i}}}{\sqrt{1-\alpha_{\tau_i}}} \right) \bar{\sigma}_{\tau_i}\epsilon \\ &\quad + \left(\sqrt{1-\alpha_{\tau_{i-1}}} - \frac{\sqrt{\alpha_{\tau_{i-1}}}\sqrt{1-\alpha_{\tau_i}}}{\sqrt{\alpha_{\tau_i}}} \right) \epsilon_\theta(\mathbf{x}_{\tau_i}, \tau_i). \end{aligned} \quad (20)$$

C. Conditional Diffusion Model

In many applications of diffusion models with classifier guidance, the unconditional score term $\nabla_{\mathbf{x}_{\tau_i}} \log p_\theta(\mathbf{x}_{\tau_i})$ can be directly computed as $-\epsilon_\theta(\mathbf{x}_{\tau_i}, \tau_i)/\sqrt{1-\alpha_{\tau_i}}$, while the calculation of the conditional score $\nabla_{\mathbf{x}_{\tau_i}} \log p_\theta(\mathbf{y}_{\tau_i}|\mathbf{x}_{\tau_i})$ in subsection III-C is very complicated. Intuitively, the conditional score term can be approximated as the difference or correction score between \mathbf{y}_{τ_i} and \mathbf{x}_{τ_i} in each denoising step, where \mathbf{y}_{τ_i} is computed by

$$\mathbf{y}_{\tau_i} = \sqrt{\alpha_{\tau_i}}\mathbf{y}_0 + \sqrt{1-\alpha_{\tau_i}}\epsilon_\theta(\mathbf{x}_{\tau_i}, \tau_i). \quad (21)$$

As a consequence, $\mathbf{y}_{\tau_i} - \mathbf{x}_{\tau_i}$ can be utilized as the likelihood to guide the deterministic data generation process of the diffusion

model. When \mathbf{y}_{τ_i} is obtained by adding noises to the raw measurements \mathbf{y}_0 contaminated by hackers or communication malfunction, the corresponding \mathbf{x}_0 generated by the reverse process will have a significant difference from \mathbf{y}_0 . As a result, the discrepancies can be considered as corrupted measurements, thus realizing the localization of the injected false data. Furthermore, when the original received data \mathbf{y}_0 only contains a small amount of corruptions, \mathbf{x}_0 synthesized by the diffusion model can be regarded as the recovery results. Collectively, according to Eq. (12), the corrected noise term can be rewritten as

$$\hat{\epsilon} = \epsilon_{\theta}(\mathbf{x}_{\tau_i}, \tau_i) - \omega \sqrt{1 - \alpha_{\tau_i}} (\mathbf{y}_{\tau_i} - \mathbf{x}_{\tau_i}), \quad (22)$$

where ω is the classifier guidance scaling parameter. When $\omega > 1$, the effect of conditional control is strong, and the measurements $\mathbf{x}_{\tau_{i-1}}$ will be quickly generated according to the expected trajectory. Nonetheless, if ω is too large, it is easy to make the synthesized reconstructed \mathbf{x}_0 the same as the input \mathbf{y}_0 , which cannot achieve the purpose of anomaly detection and measurement recovery. To this end, the conditioned diffusion model should choose an appropriate ω for different scale power systems by conducting recovery error tests under different ω .

D. Diffusion-Based Imputation

This subsection utilizes the diffusion model to complement the missing positions by aforementioned reasons in subsection II-B. Denote the index set of correctly observed data points as Ω , and the index set of abnormal or unobserved data points as $1 - \Omega$. In this way, the known measurements can be represented as $\Omega \odot \mathbf{x}$, and the unidentified data can be described as $(1 - \Omega) \odot \mathbf{x}$. Evidently, in every iteration of the reconstruction process, the normal measurements should remain unchanged, while the missing entries will be imputed by the generated data. The distribution of imputation part of data and the combined data can be expressed as

$$\begin{aligned} \mathbf{x}_{\tau_{i-1}}^{\Omega} &\sim \mathcal{N}(\sqrt{\alpha_{\tau_{i-1}}} \mathbf{x}_0, (1 - \alpha_{\tau_{i-1}}) \mathbf{I}) \\ \mathbf{x}_{\tau_{i-1}}^{(1-\Omega)} &\sim \mathcal{N}(\bar{\mu}(\mathbf{x}_{\tau_i}), \gamma_{\tau_i}^2 \bar{\sigma}_{\tau_i}^2 \mathbf{I}) \\ \mathbf{x}_{\tau_{i-1}} &= \Omega \odot \mathbf{x}_{\tau_{i-1}}^{\Omega} + (1 - \Omega) \odot \mathbf{x}_{\tau_{i-1}}^{(1-\Omega)}. \end{aligned} \quad (23)$$

Additionally, in order to achieve better coordination between generated measurements and the normal observations, resampling is an appropriate enhancement method to obtain more coordinated results. In detail, \mathbf{x}_{τ_i} is obtained again by adding noises based on the denoising data $\mathbf{x}_{\tau_{i-1}}$, which can be represented as

$$\mathbf{x}_{\tau_i} = \sqrt{1 - \beta_{\tau_i}} \mathbf{x}_{\tau_{i-1}} + \sqrt{\beta_{\tau_i}} \epsilon, \quad (24)$$

where $\epsilon \sim \mathcal{N}(0, \mathbf{I})$. Subsequently, the reverse process is performed on \mathbf{x}_{τ_i} again to compute $\mathbf{x}_{\tau_{i-1}}$. The proposed improved diffusion model will repeat the above resampling process by R times to pursue higher accuracy and reliability.

E. Improved Two-Stage Diffusion Recovery Model

The proposed improved diffusion model is implemented based on the denoising U-Net. The denoising U-Net is an artificial neural network with an autoencoder architecture combined with a residual block and an attention block. The

optimization objective of the denoising U-Net is to make the predicted noises ϵ_{θ} consistent with the real noises ϵ , i.e., denoising U-Net randomly selects a normal sample and step n during training process, and then calculates the L_2 loss between ϵ_{θ} and ϵ to update the gradient and network. Moreover, the U-Net encodes step n into the network in a time embedding manner.

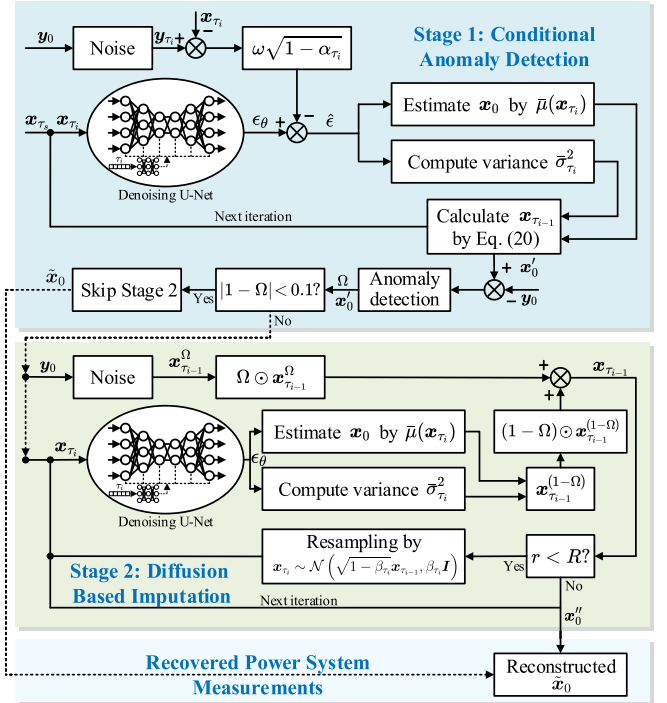


Fig. 3. The flowchart of improved efficient TSDM with Stage 1: conditional anomaly detection and Stage 2: diffusion based imputation.

The unreasonable setting of ω in different scenarios and the possible existence of massive false data and data losses will have a negative impact on restored data of the diffusion model, and \mathbf{y}_{τ_i} cannot effectively guide the precise data generation process. To this end, as illustrated in Fig. 3 and Algorithm 1, the improved TSDM proposed in this paper consists of two stages: Stage 1 comprises a classifier-guided conditional anomaly detection model, which first uses the conditional diffusion technique discussed in subsection IV-C to recover a data matrix $\mathbf{x}'_0 \in \mathbb{R}^{M \times T}$ and then computes the difference between \mathbf{x}'_0 and the corrupted power system measurement matrix \mathbf{y}_0 . Suspected outliers in \mathbf{y}_0 are then identified by performing 3σ tests [20] on the standard deviations. If the proportion of suspected outliers is less than 10%, \mathbf{x}'_0 can be directly regarded as the output data $\tilde{\mathbf{x}}_0$. Otherwise, the index set $1 - \Omega$ of the suspected outliers is sent to Stage 2 with the same denoising U-Net, where the diffusion-based imputation discussed in subsection IV-D is used to restore the missing data and finally produce the output $\tilde{\mathbf{x}}_0$. In addition, the two-stage diffusion model utilizes DDIM and optimal variance acceleration strategy to achieve efficient data recovery.

F. Cyber-Physical Implementation of TSDM

As illustrated in Fig. 4, on the one hand, modern power systems estimate the static state \mathbf{s}_t^U at time t in control

Algorithm 1: Improved efficient two-stage denoising diffusion measurement recovery model

Input: Measurements matrix $\mathbf{y}_0 \in \mathbb{R}^{M \times T}$, variance schedule $\{\beta_n\}_{n=1}^N$ and $\{\alpha_n\}_{n=1}^N$, subsequence $\tau = [\tau_1, \tau_2, \dots, \tau_s]$, guidance scaling parameter ω , resampling parameter R

Output: Restored measurements matrix $\tilde{\mathbf{x}}_0$

```

1 Initialize  $\mathbf{x}$  by  $\mathbf{x}_{\tau_s} \sim \mathcal{N}(0, \mathbf{I})$ ;
2 Stage 1:
3 for all  $i = s, \dots, 2$  do
4   Compute noisy data  $\mathbf{y}_{\tau_i} \leftarrow \sqrt{\alpha_{\tau_i}} \mathbf{y}_0 + \sqrt{1 - \alpha_{\tau_i}} \epsilon_{\theta}(\mathbf{x}_{\tau_i}, \tau_i)$ ;
5   Rectify noise term  $\hat{\epsilon} \leftarrow \epsilon_{\theta}(\mathbf{x}_{\tau_i}, \tau_i) - \omega \sqrt{1 - \alpha_{\tau_i}} (\mathbf{y}_{\tau_i} - \mathbf{x}_{\tau_i})$ ;
6   Estimate  $\mathbf{x}_0$  by  $\bar{\mu}(\mathbf{x}_{\tau_i}) \leftarrow \frac{1}{\sqrt{\alpha_{\tau_i}}} [\mathbf{x}_{\tau_i} - \sqrt{1 - \alpha_{\tau_i}} \hat{\epsilon}]$ ;
7   Compute optimal variance by
    $\bar{\sigma}_{\tau_i}^2 \leftarrow \frac{1 - \alpha_{\tau_i}}{\alpha_{\tau_i}} \left\{ 1 - \frac{1}{d} \mathbb{E}_{\mathbf{x}_{\tau_i} \sim p(\mathbf{x}_{\tau_i})} [\|\hat{\epsilon}\|_2^2] \right\}$ ;
8   Update  $\mathbf{x}_{\tau_{i-1}}$  by Eq. (19) using  $\bar{\mu}(\mathbf{x}_{\tau_i})$  and  $\bar{\sigma}_{\tau_i}^2$ ;
9 end
10 Estimate  $\mathbf{x}_0$  by  $\mathbf{x}'_0 \leftarrow \frac{1}{\sqrt{\alpha_{\tau_1}}} [\mathbf{x}_{\tau_1} - \sqrt{1 - \alpha_{\tau_1}} \hat{\epsilon}]$ ;
11 Find the outlier positions by  $(1 - \Omega) \leftarrow (|\mathbf{x}'_0 - \mathbf{y}_0| > 3\sigma_{\mathbf{y}_0})$ ;
12 if the proportion of outliers meets  $|1 - \Omega| < 0.1$  then
13   Output  $\tilde{\mathbf{x}}_0 \leftarrow \mathbf{x}'_0$  and Skip Stage 2;
14 end
15 Stage 2:
16 for all  $i = s, \dots, 2$  do
17   for  $r = 1, \dots, R$  do
18     Compute known  $\mathbf{x}_{\tau_{i-1}}^{\Omega} \leftarrow \sqrt{\alpha_{\tau_{i-1}}} \mathbf{y}_0 + \sqrt{1 - \alpha_{\tau_{i-1}}} \epsilon_1$ ;
19     Estimate  $\mathbf{x}_0$  by
      $\bar{\mu}(\mathbf{x}_{\tau_i}) \leftarrow \frac{1}{\sqrt{\alpha_{\tau_i}}} [\mathbf{x}_{\tau_i} - \sqrt{1 - \alpha_{\tau_i}} \epsilon_{\theta}(\mathbf{x}_{\tau_i}, \tau_i)]$ ;
20     Compute optimal variance by
      $\bar{\sigma}_{\tau_i}^2 \leftarrow \frac{1 - \alpha_{\tau_i}}{\alpha_{\tau_i}} \left\{ 1 - \frac{1}{d} \mathbb{E}_{\mathbf{x}_{\tau_i} \sim p(\mathbf{x}_{\tau_i})} [\|\epsilon_{\theta}(\mathbf{x}_{\tau_i}, \tau_i)\|_2^2] \right\}$ ;
21     Update  $\mathbf{x}_{\tau_{i-1}}^{(1-\Omega)}$  by Eq. (20) using  $\bar{\mu}(\mathbf{x}_{\tau_i})$  and  $\bar{\sigma}_{\tau_i}^2$ ;
22     Combine by  $\mathbf{x}_{\tau_{i-1}} \leftarrow \Omega \odot \mathbf{x}_{\tau_{i-1}}^{(1-\Omega)} + (1 - \Omega) \odot \mathbf{x}_{\tau_{i-1}}^{\Omega}$ ;
23     if  $r < R$  then
24       Resample  $\mathbf{x}_{\tau_i} \leftarrow \sqrt{1 - \beta_{\tau_i}} \mathbf{x}_{\tau_{i-1}} + \sqrt{\beta_{\tau_i}} \epsilon_2$ ;
25     end
26   end
27 end
28 Estimate  $\mathbf{x}_0$  by  $\mathbf{x}''_0 \leftarrow \Omega \odot \sqrt{\alpha_{\tau_1}} \mathbf{y}_0 + (1 - \Omega) \odot \bar{\mu}(\mathbf{x}_{\tau_1})$ ;
29 Return reconstructed  $\tilde{\mathbf{x}}_0 \leftarrow \mathbf{x}''_0$ 

```

center, and on the other hand, monitor the dynamic transients through WAMS. Measurements $\mathbf{z}_t^{\mathcal{U}}$ collected by PMU and RTU during data transmission may be injected with false data $\Delta(\mathbf{z}_t^{\mathcal{U}})$ by hackers, and data losses may also occur due to communication malfunction and latencies, resulting in a corrupted or unobserved estimated state $(\mathbf{s}_t^{\mathcal{U}})^{\mathcal{U}}$. The proposed TSDM can rectify biased state variables through $\tilde{\mathbf{s}}_t^{\mathcal{U}} = \arg \min_{\tilde{\mathbf{s}}_t^{\mathcal{U}}} \|f_{\text{TSDM}}^s((\mathbf{z}_t^{\mathcal{U}})^{\mathcal{U}}) - h^{\mathcal{U}}(\tilde{\mathbf{s}}_t^{\mathcal{U}})\|_0$ by considering SCADA measurement equation constraints in power system area \mathcal{U}

$$\begin{aligned}
 P_i &= U_i \sum_{j \in \mathcal{R}_i} U_j (G_{ij} \cos \theta_{ij} + B_{ij} \sin \theta_{ij}) \\
 Q_i &= U_i \sum_{j \in \mathcal{R}_i} U_j (G_{ij} \sin \theta_{ij} - B_{ij} \cos \theta_{ij}) \\
 P_{ij} &= U_i^2 (g_{ij} + g_{i0}) - U_i U_j (g_{ij} \cos \theta_{ij} + b_{ij} \sin \theta_{ij}) \\
 Q_{ij} &= -U_i^2 (b_{ij} + b_{i0}) + U_i U_j (b_{ij} \cos \theta_{ij} - g_{ij} \sin \theta_{ij}), \quad (25)
 \end{aligned}$$

where $f_{\text{TSDM}}^s(\cdot)$ is the nonlinear function of TSDM with a s -length subsequence. SCADA measurements include active/reactive power injection P_i/Q_i , active/reactive power flow P_{ij}/Q_{ij} , and bus magnitude U_i . Moreover, θ_{ij} is the phase angle difference between Buses i and j , $G_{ij} + B_{ij}$ is the ij -th element of the admittance matrix, $g_{ij} + b_{ij}$ is the admittance of

the line connecting Buses i and j , $g_{i0} + b_{i0}$ is the admittance of the shunt branch of Bus i , \mathcal{R}_i represents the bus indexes that are connected to Bus i . In WAMS, the following state-transition and measurement equation constraints

$$\begin{aligned}
 \dot{\delta}_{Gi} &= \Delta\omega_{Gi}, 2H_{Gi}\Delta\dot{\omega}_{Gi} = P_{mGi} - P_{Gi} - D_{Gi}\Delta\omega_{Gi} \\
 T'_{qGi0}\dot{E}'_{dGi} &= -E'_{dGi} - (X_{qGi} - X'_{qGi})I_{qGi} \\
 T'_{dGi0}\dot{E}'_{qGi} &= E_{fdGi} - E'_{qGi} - (X_{dGi} - X'_{dGi})I_{dGi} \\
 \begin{bmatrix} U_{dGi} \\ U_{qGi} \end{bmatrix} &= \begin{bmatrix} \sin(\delta_{Gi}) & -\cos(\delta_{Gi}) \\ \cos(\delta_{Gi}) & \sin(\delta_{Gi}) \end{bmatrix} \begin{bmatrix} U_i \cos(\theta_i) \\ U_i \sin(\theta_i) \end{bmatrix} \\
 U_{dGi} &= E'_{dGi} + I_{qGi}X'_{qGi} - R_{aGi}I_{dGi} \\
 U_{qGi} &= E'_{qGi} - I_{dGi}X'_{dGi} - R_{aGi}I_{qGi} \\
 P_{Gi} &= U_{dGi}I_{dGi} + U_{qGi}I_{qGi}, Q_{Gi} = U_{qGi}I_{dGi} - U_{dGi}I_{qGi} \\
 I_i^2 &= I_{dGi}^2 + I_{qGi}^2, \gamma_i = \tan^{-1}(-I_{dGi}/I_{qGi}) + \delta_{Gi} \quad (27)
 \end{aligned}$$

are also considered, where δ_{Gi} is the power angle, ω_{Gi} is the rotor speed, H_{Gi} is the inertia constant, P_{mGi} is the mechanical input power, D_{Gi} is the damping coefficient, T'_{qGi0} and T'_{dGi0} are the d-axis and q-axis transient time constants, E'_{dGi} and E'_{qGi} are the d-axis and q-axis transient voltages, E_{fdGi} is the field voltage, X_{dGi} and X_{qGi} are d-axis and q-axis synchronous reactances, X'_{dGi} and X'_{qGi} are d-axis and q-axis transient reactances, U_{dGi}/U_{qGi} and I_{dGi}/I_{qGi} are the d-axis and q-axis voltage and current respectively, and R_a is the stator series resistance. WAMS measurements from the PMU installed at the generator terminal bus include generator active/reactive power output P_{Gi}/Q_{Gi} , voltage/current magnitude U_i/I_i and phase angle θ_i/γ_i .

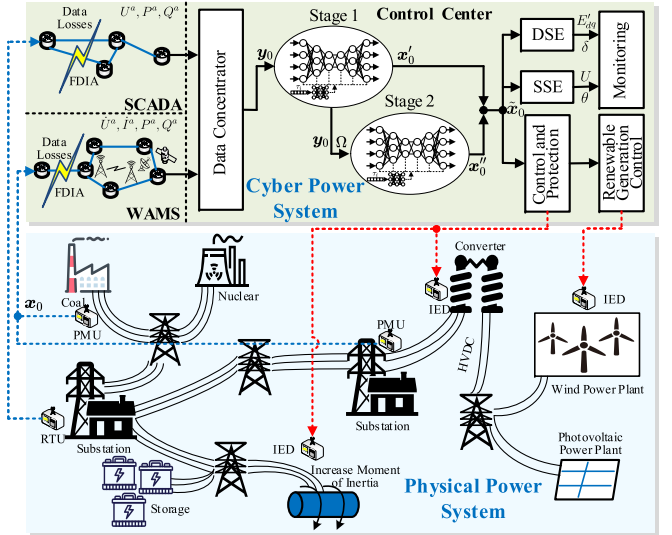


Fig. 4. Procedures and applications of the proposed TSDM algorithm.

SSE/DSE in control center can estimate the states $\mathbf{s}_t^{\mathcal{U}} = [U_i, \theta_i]^T$ or $\mathbf{s}_t^{\mathcal{U}} = [\delta_{Gi}, \omega_{Gi}, E'_{dGi}, E'_{qGi}]^T$ based on the input measurements. The proposed TSDM can eliminate the impact of contaminated data $\hat{U}^a, \hat{I}^a, P^a, Q^a$ and obtain accurate system static or dynamic states $\tilde{\mathbf{s}}_t^{\mathcal{U}}$. Eventually, the rectified $\tilde{\mathbf{x}}_0$ and state variables $\tilde{\mathbf{s}}_t^{\mathcal{U}}$ are utilized by modern power systems as the data support for monitoring, protection, and control, facilitating the safety and stability of complex, highly nonlinear power systems with measurement uncertainties.

V. CASE STUDIES

A. Experimental Setup

Dataset Source: Two typical application scenarios, i.e., the RTU-based SCADA system and the PMU-based WAMS, are implemented for case studies. For the SCADA scenario, training and test data of IEEE 30, 57, and 118-bus systems is obtained via simulation on MATPOWER 7.0. The load data are extracted from [21]. Furthermore, parts of generation profiles are replaced with actual renewable power output from January 2022 to June 2023 in Belgium [22]. The load and renewables output curve for a certain week is illustrated in Fig. 5. The data reporting rate is set to 1 sample per 15 minutes. For the WAMS scenario, transient data of IEEE 39-bus and NPCC 140-bus systems are obtain using the open-source simulator Python-based ANDES [23]. PMUs are installed at 13 optimal locations in IEEE 39-bus system [24] and 30 generator terminal buses in NPCC 140-bus system [25], with a reporting rate of 30 Hz. Five thousand different power system events, including short-circuit faults, line trips, generator sheddings, and load changes, are considered in the simulation.

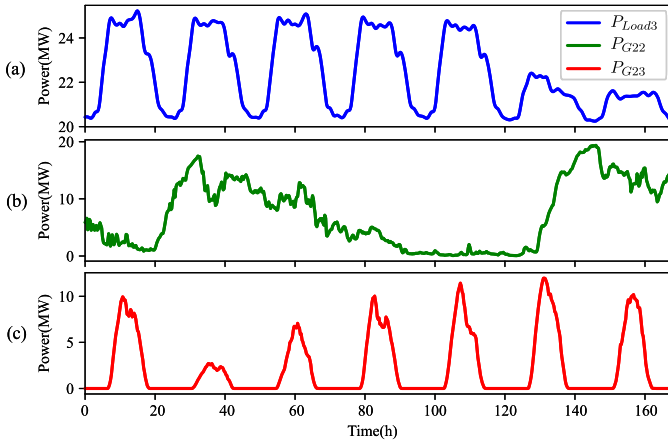


Fig. 5. The weekly commercial active power demand of load 3 (a), power output of wind turbines 22 (b), and power output of photovoltaic generators 23 (c) of IEEE 30-bus test system .

Model Training: An independent TSDM is trained for each test system based on Pytorch 1.8.1. The total timesteps and DDIM subsequence lengths are uniformly set to $N=100$ and $s=10$, respectively. Meanwhile, LSTM, variational auto-encoder (VAE), and GAN are also trained for comparison, where the structure of the GAN follows the optimized Wasserstein GAN (WGAN) with an additional encoder. The simulations run in MATLAB R2021a and Python 3.8.6 on a computer with an i7-8700U 3.2 GHz CPU and 16 GB of RAM.

Performance Metrics: Weighted root mean squared error (RMSE) is utilized to verify the state reconstruction accuracy

$$\begin{aligned} \text{RMSE} &= \|\mathbf{m} (s_{1:T}^{\mathcal{U}} - \tilde{s}_{1:T}^{\mathcal{U}})\|_2 \\ &= \sqrt{\frac{1}{S \times T} \sum_{i=1}^S m_i \sum_{j=1}^T (s_{ij}^{\mathcal{U}} - \tilde{s}_{ij}^{\mathcal{U}})^2}, \end{aligned} \quad (28)$$

where $s_{ij}^{\mathcal{U}}$ and $\tilde{s}_{ij}^{\mathcal{U}}$ are the actual and restored state elements, and m_i is the weight coefficient of the i -th state variable.

B. Steady-State Recovery of SCADA Measurements

TSDM and GAN are first tested using the SCADA data from the IEEE 30-bus test system. The models are trained using the measurements of 2022, and are tested with the data from 6 am to 4 pm on Jan. 1, 2023. In the test data, step attacks are applied to 20% of state variables, with the attack amplitude equal to 2.5% for voltage magnitudes and 50% for phase angles. The original and corrupted state estimates at 10 am, as well as the state estimates restored by TSDM and GAN, are shown in Fig. 6. It can be seen that the proposed TSDM achieves a higher data recovery accuracy, and the predicted output is generally consistent with the original state estimates. On the other hand, GAN still shows non-negligible deviations from the expected values, although the deviations have already been suppressed to some extent.

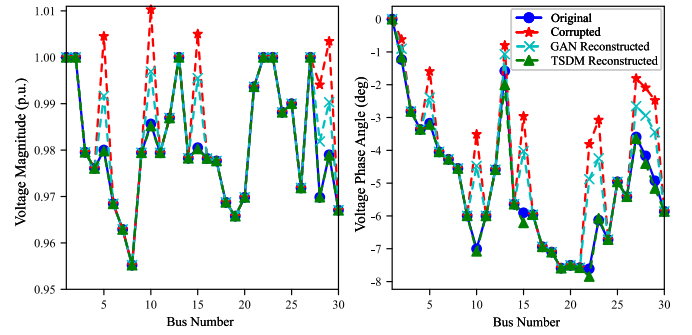


Fig. 6. The estimated state variables corrupted by step attacks and reconstructed by TSDM and GAN in IEEE 30-bus system.

The second test assumes an NM data loss scenario between 8 am and 6 pm, where 30% of the measurements in the IEEE 57-bus system cannot reach the control center. The original and corrupted state estimates at 10 am, as well as the state estimates recovered by the two models, are shown in Fig. 7. Similar to the results above, TSDM apparently has smaller data imputation errors than GAN.

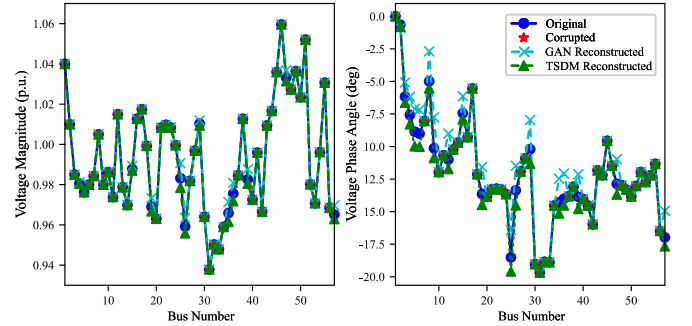


Fig. 7. The estimated state variables corrupted by NM and reconstructed by TSDM and GAN in IEEE 57-bus system.

For the large-scale 118-bus system, random FDIAs with zero mean, magnitude variance of 0.03, and phase angle variance of 0.6 are applied to 30% of the state variables from 6 am to 8 pm. The original and corrupted state estimates and the estimates obtained based on restored data are shown in Fig. 8. Again, state variables can be accurately estimated using the data reconstructed by TSDM. However, GAN-restored data lead to a significant bias in phase angle estimation.

TABLE I
WEIGHTED RMSE OF IEEE 30-BUS, 57-BUS, AND 118-BUS IN STEADY-STATE RECOVERY VIA FIVE METHODS

Test System		IEEE 30-bus					IEEE 57-bus					IEEE 118-bus				
Anomalies	Method	LSTM	ADMM	VAE	GAN	TSDM	LSTM	ADMM	VAE	GAN	TSDM	LSTM	ADMM	VAE	GAN	TSDM
FDIA	Step	4.58	3.66	2.32	2.22	0.77	4.27	3.80	3.83	2.38	0.78	13.45	6.15	3.66	3.09	1.28
	Ramp	4.19	3.52	2.42	1.61	0.55	4.23	3.70	3.91	2.09	0.72	11.44	6.07	3.63	2.99	1.26
	Random	3.53	2.61	2.31	1.98	0.42	4.27	2.07	3.72	2.67	0.57	13.45	6.32	3.48	2.93	1.14
Data Loss	RM	4.35	0.56	3.48	3.11	0.14	3.49	0.39	3.99	2.86	0.39	3.71	0.47	3.63	3.12	0.23
	NM	2.20	0.65	3.54	2.51	0.30	2.92	0.39	3.98	2.19	0.15	3.37	0.51	3.60	3.48	0.14

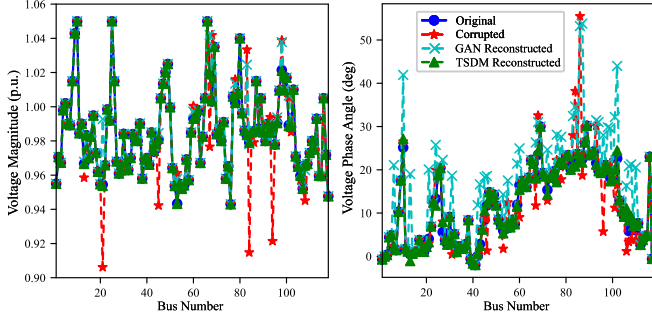


Fig. 8. The estimated state variables corrupted by random FDIA and reconstructed by TSDM and GAN in IEEE 118-bus system.

Numerical recovery experiments are carried out in different scenarios to verify the proposed TSDM. The test data include SCADA measurements sampled from January to June 2023 contaminated by step/ramp/random FDIA and RM/NM data loss with attack region modified ratios of 1% to 50%. The magnitude and phase angle attack amplitudes are 1%-10% and 10%-100%, respectively. The algorithms for comparison include the time-series model LSTM [9], ADMM based robust principal component analysis and matrix completion mathematical algorithms [14], [15], and reconstruction networks Gaussian mixture model based VAE [26] and Encoder-WGAN [4]. Table I shows that the time-series models represented by LSTM have difficulty in accurately predicting the quasi-steady measurement changes in modern power systems with renewable energy integration. Moreover, ADMM has a significant RMSE in FDIA data recovery tasks, and the RMSE of two typical reconstruction algorithms VAE and GAN are much greater than that of the proposed TSDM.

C. Dynamic Recovery of PMU Measurements

To demonstrate the performance of TSDM in complex nonlinear dynamics, PMU data under a series of power system events are used in this set of tests. In the first case, a three-phase fault with grounding reactance $x_f=0.075$ p.u. occurs at 1s near Bus 5 of the NPCC 140-bus system and is cleared at 1.06s, and Line 5 between Buses 5 and 6 is disconnected at 1.05s and recloses at 1.104s. Moreover, a replay attack is applied during 11s-20s. The measurements of Bus 22 restored by GAN and TSDM are illustrated in Fig. 9. It can be seen that the output of TSDM gradually converges to the states along the iteration steps of 96, 46, 21, and 1 of the underlying DDPM model, while the GAN output is significantly affected by the contingencies.

In the second case, Line 11 between Buses 6 and 7 and Line 28 between Buses 22 and 23 in the IEEE 39-bus system are

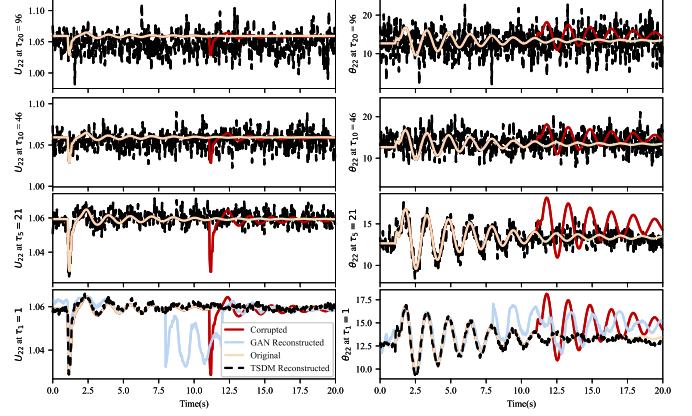


Fig. 9. Data recovery results of GAN and TSDM against a replay attack during a three phase fault.

disconnected from 1s to 1.06s, with an NM data loss applied during 0s-12s. The measurements of Generator 2 during the line trips restored by GAN and TSDM are illustrated in Fig. 10. It can be seen that the missing entries of the power angle δ_{G2} and q-axis transient voltage E'_{qG2} of Generator 2 gradually approach the actual values during the guided conditional denoising process of TSDM. However, the recovery accuracy of GAN is slightly worse.

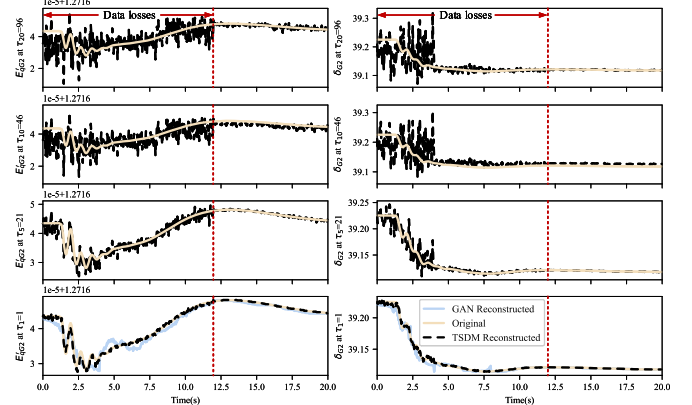


Fig. 10. Data recovery results of GAN and TSDM against data loss during line trips.

The third case assumes a composite attack scenario to verify the recovery effectiveness of TSDM. In this case, a 68 MW load is disconnected to Bus 35 during 1s-1.05s, with random noises of zero mean and 0.3 variance, a 30% step attack, an 80% ramp attack, and a 50% amplitude scaling attack applied to the transient d-axis voltage E'_{dG5} , power angle δ_{G5} , bus voltage magnitude V_2 , and phase angle θ_2 , respectively. Fig. 11 indicates that TSDM can still effectively restore the highly nonlinear dynamics in such a complex FDIA scenario.

TABLE II
WEIGHTED RMSE OF IEEE 39-BUS AND NPCC 140-BUS IN DYNAMIC-STATE RECOVERY VIA FIVE METHODS

Test System		IEEE 39-bus					NPCC 140-bus				
Anomalies	Method	LSTM	ADMM	VAE	GAN	TSDM	LSTM	ADMM	VAE	GAN	TSDM
	FDIA	Step	3.07	2.67	1.01	0.42	0.20	3.67	3.41	1.40	0.68
Ramp		3.08	2.09	1.03	0.31	0.19	3.43	3.32	1.41	0.78	0.34
Random		2.97	3.04	1.01	0.74	0.22	3.12	2.90	1.38	0.55	0.31
Data Loss	RM	3.40	0.53	1.15	0.47	0.14	3.80	0.36	2.23	1.45	0.21
	NM	3.25	0.55	1.87	1.10	0.10	3.88	0.31	2.15	1.40	0.14

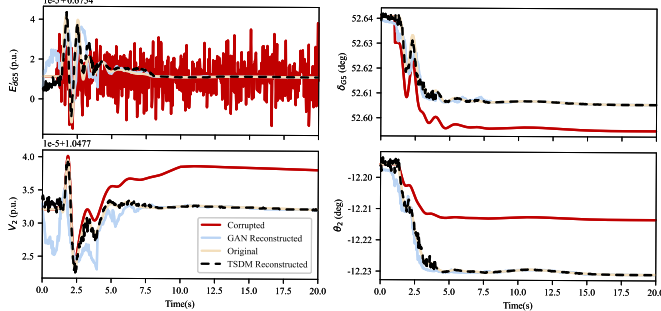


Fig. 11. Data recovery results of GAN and TSDM against a composite FDIA during a load change.

Similarly, TSDM can accurately recover measurements and ensure state estimation accuracy in generator trip events in Fig. 12 and the scenario of phase shift attacks in Fig. 13. More typical reconstruction results and cases of highly non-linear dynamics can be found in the Appendix.

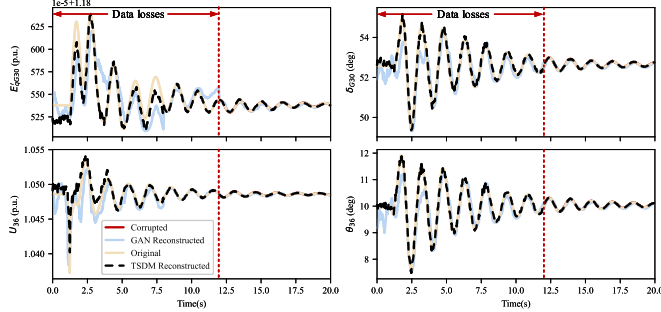


Fig. 12. Data recovery results of GAN and TSDM against data loss during a generator shedding.

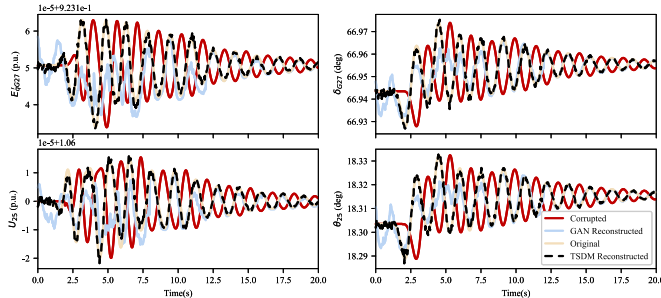


Fig. 13. Data recovery results of GAN and TSDM against 180° phase shift attack during a line trip.

The test data of the numerical verification are the WAMS measurements collected during different power system contingencies not included in the training datasets. The modified ratios are 1% to 50%. In Table II, the proposed TSDM still maintains and demonstrates strong superiority in power grid

dynamics, with RMSE smaller than existing methods in both FDIA reconstruction tasks and unobservable state variables complementation.

D. Hyperparameter Selection

It is necessary to select appropriate values of the hyperparameters ω in Stage 1 and R in Stage 2. In this experiment, ω and R are adjusted between $[0.1, 2.0]$ and $[1, 10]$, respectively, to determine the optimal values. The test dataset for ω contains outliers caused by step, ramp, and random attacks, while the dataset for R contains RM and NM data loss. The average weighted RMSE is shown in Fig. 14. It can be seen that the recovery error increases with the expansion of the system scale. Meanwhile, steady-state data recovery tends to have larger error than dynamic data recovery. In the guided conditional denoising diffusion process of Stage 1, as ω gradually increases, the diffusion generation trajectory of TSDM gradually shifts from random to deterministic, and the recovery error gradually decreases. Nonetheless, when ω is too large, the generation result is exactly the same as the original contaminated measurements y_0 , and the recovery error increases. In this way, it is appropriate to set $\omega=1.0$. In the diffusion-based imputation process of Stage 2, a larger R will result in smaller errors but higher computational complexity. To this end, R is set to 2.

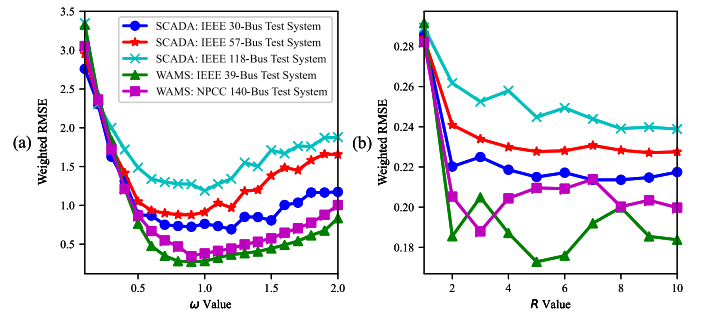


Fig. 14. The weighted RMSE under different (a) ω and (b) R .

E. Robustness on FDIA and Data Losses

TSDM can also maintain better robustness in different scenarios. To verify this, the reconstruction errors of VAE, GAN, and TSDM algorithms are calculated at a modified ratio of 1%-50%, as illustrated in Fig. 15. It can be seen that the data recovery error of various algorithms gradually increases as the proportion of anomalies increases. Nonetheless, the robustness performance of TSDM is better than the other two commonly used reconstruction algorithms. The proposed two-stage strategy effectively improves the robustness of TSDM.

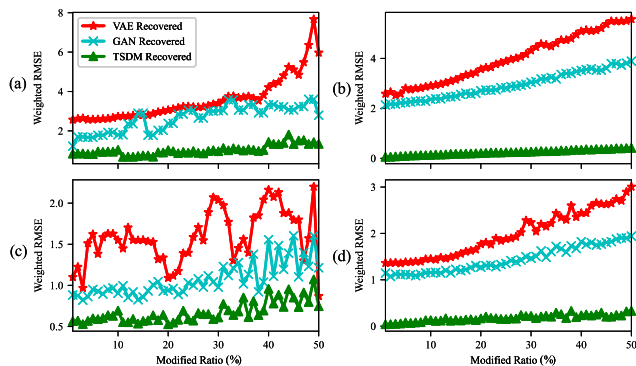


Fig. 15. SCADA FDIA (a) and data losses (b), WAMS FDIA (c) and data losses (d) recovery RMSE with different modified ratios.

TABLE III

THE RECOVERY ERROR AND TIME CONSUMPTION OF DDPM, DDIM, AND TSDM (WEIGHTED RMSE / TIME CONSUMPTION (SECOND))

Data type $M \times T$	Model	Subsequence Length			
		$s=10$	$s=20$	$s=50$	$s=100$
SCADA: IEEE 30-bus 24×96	DDPM	-	-	-	4.35/9.22
	DDIM	1.30/0.94	0.89/1.85	0.74/4.79	0.68/9.14
	TSDM	0.69/0.91	0.66/1.81	0.65/4.49	0.64/9.19
SCADA: IEEE 57-bus 48×96	DDPM	-	-	-	4.30/17.61
	DDIM	1.37/1.77	1.01/3.56	0.84/8.91	0.79/17.43
	TSDM	0.82/1.76	0.79/3.47	0.78/8.80	0.76/17.59
SCADA: IEEE 118-bus 96×96	DDPM	-	-	-	5.29/36.07
	DDIM	1.35/3.53	1.00/7.13	0.86/18.09	0.83/35.35
	TSDM	0.81/3.63	0.79/7.05	0.77/17.90	0.76/35.99
WAMS: IEEE 39-bus 48×120	DDPM	-	-	-	4.75/21.43
	DDIM	1.18/2.18	0.79/4.35	0.51/10.87	0.41/21.62
	TSDM	0.43/2.23	0.39/4.44	0.36/10.91	0.34/21.75
WAMS: NPPC 140-bus 120×120	DDPM	-	-	-	3.87/51.02
	DDIM	1.20/5.16	0.81/10.44	0.57/25.79	0.51/51.31
	TSDM	0.53/5.21	0.48/10.59	0.45/26.09	0.44/51.36

F. Timeliness with Acceleration Strategy

DDIM with precise estimated mean and optimal variance is one of the contributions of TSDM, which can effectively mitigate one of the drawbacks of diffusion models, i.e., more prolonged time consumption than some commonly used AI models. The time consumption and weighted RMSE of DDPM with original timestep length, DDIM with different subsequence lengths, and TSDM algorithm with optimal variance in different test systems with attack region measurement dimensionality ($M \times T$) are shown in Table III. The diffusion generation process of the original DDPM is completely random and cannot be directly applied to measurement rectification or state reconstruction, resulting in significant recovery errors. However, under the same subsequence length, the reconstruction RMSE of TSDM is much lower than the original conditional DDIM. Meanwhile, under the same reconstruction precision, the time consumption of TSDM is much less (about 10%) than that of the original diffusion models. Moreover, the proposed TSDM can flexibly partition attack areas of a power system and reduce data dimensionality to achieve faster data recovery.

VI. CONCLUSION

This paper proposes an improved two-stage power system measurement recovery model (TSDM) based on denoising diffusion models. The proposed TSDM can effectively extract the spatio-temporal correlations and measurement coordinations

between data points and use the extracted patterns to guide the process of outlier elimination and missing data supplementation. Compared with existing reconstruction methods, the proposed model demonstrates high recovery accuracy and strong robustness under highly random and nonlinear dynamics of power systems. This is evidenced through extensive case studies based on SCADA and WAMS data. Nonetheless, the exploration of real-time data recovery leveraging denoising diffusion models warrants further investigation.

REFERENCES

- [1] E. R. Fernandes, S. G. Ghiocel, and J. H. Chow, "Application of a phasor-only state estimator to a large power system using real pmu data," *IEEE Trans. Power Syst.*, vol. 32, no. 1, pp. 411–420, 2017.
- [2] S. Pal, B. Sikdar, and J. H. Chow, "Classification and detection of pmu data manipulation attacks using transmission line parameters," *IEEE Trans. Smart Grid*, vol. 9, no. 5, pp. 5057–5066, 2018.
- [3] S. Wei, J. Xu, and Z. Wu, "A false data injection attack detection strategy for unbalanced distribution networks state estimation," *IEEE Trans. Smart Grid*, vol. 14, no. 5, pp. 3992–4006, 2023.
- [4] Y. Li, Y. Wang, and S. Hu, "Online generative adversary network based measurement recovery in false data injection attacks: A cyber-physical approach," *IEEE Trans. Ind. Informat.*, vol. 16, no. 3, pp. 2031–2043, 2020.
- [5] H. Wang, X. Wen, Y. Xu, and B. Zhou, "Operating state reconstruction in cyber physical smart grid for automatic attack filtering," *IEEE Trans. Ind. Informat.*, vol. 18, no. 5, pp. 2909–2922, 2022.
- [6] T. Wu, W. Xue, and H. Wang, "Extreme learning machine-based state reconstruction for automatic attack filtering in cyber physical power system," *IEEE Trans. Ind. Informat.*, vol. 17, no. 3, pp. 1892–1904, 2021.
- [7] J. Ruan, G. Liang, J. Zhao, J. Qiu, and Z. Y. Dong, "An inertia-based data recovery scheme for false data injection attack," *IEEE Trans. Ind. Informat.*, vol. 18, no. 11, pp. 7814–7823, 2022.
- [8] Z. Yang, H. Liu, and T. Bi, "An adaptive pmu missing data recovery method," *Int. J. Elec. Power*, vol. 116, p. 105577, 2020.
- [9] J. J. Q. Yu, A. Y. S. Lam, and D. J. Hill, "Delay aware power system synchrophasor recovery and prediction framework," *IEEE Trans. Smart Grid*, vol. 10, no. 4, pp. 3732–3742, 2019.
- [10] J. J. Q. Yu, D. J. Hill, V. O. K. Li, and Y. Hou, "Synchrophasor recovery and prediction: A graph-based deep learning approach," *IEEE Internet Things J.*, vol. 6, no. 5, pp. 7348–7359, 2019.
- [11] P. Gao, M. Wang, and J. H. Chow, "Missing data recovery by exploiting low-dimensionality in power system synchrophasor measurements," *IEEE Trans. Power Syst.*, vol. 31, no. 2, pp. 1006–1013, 2016.
- [12] J. Pei, J. Wang, Z. Wang, and D. Shi, "Precise recovery of corrupted synchrophasors based on autoregressive bayesian low-rank factorization and adaptive k-medoids clustering," *IEEE Trans. Power Syst.*, vol. 38, no. 6, pp. 5834–5848, 2023.
- [13] M. Wang, J. H. Chow, and D. Osipov, "Review of low-rank data-driven methods applied to synchrophasor measurement," *IEEE Open Access Journal of Power and Energy*, vol. 8, pp. 532–542, 2021.
- [14] K. Mahapatra and N. R. Chaudhuri, "Malicious corruption-resilient wide-area oscillation monitoring using principal component pursuit," *IEEE Trans. Smart Grid*, vol. 10, no. 2, pp. 1813–1825, 2019.
- [15] M. Liao, D. Shi, and Z. Yu, "An alternating direction method of multipliers based approach for pmu data recovery," *IEEE Trans. Smart Grid*, vol. 10, no. 4, pp. 4554–4565, 2019.
- [16] J. Ho, A. Jain, and P. Abbeel, "Dennoising diffusion probabilistic models," in *34th Conference on Neural Information Processing Systems (NeurIPS)*, Vancouver, Canada, Dec. 2020, pp. 1–25.
- [17] J. Song, C. Meng, and S. Ermon, "Dennoising diffusion implicit models," in *International Conference on Learning Representations (ICLR)*, Online, May 2021, pp. 1–22.
- [18] J. Zhao, Z. Zheng, and S. Wang, "Correlation-aided robust decentralized dynamic state estimation of power systems with unknown control inputs," *IEEE Trans. Power Syst.*, vol. 35, no. 3, pp. 2443–2451, 2020.
- [19] T. K. Chau, S. Yu, T. L. Fernando, and H. H.-C. Iu, "An adaptive-phasor approach to pmu measurement rectification for Ifoed enhancement," *IEEE Trans. Power Syst.*, vol. 34, no. 5, pp. 3941–3950, 2019.
- [20] C. C. Aggarwal, *Outlier analysis second edition*. Springer Switzerland, 2016.
- [21] H. Li, J. H. Yeo, and A. L. Bornsheuer, "The creation and validation of load time series for synthetic electric power systems," *IEEE Trans. Power Syst.*, vol. 36, no. 2, pp. 961–969, 2021.
- [22] J.-F. Toubeau and J. Bottieau, "Data-driven scheduling of energy storage in day-ahead energy and reserve markets with probabilistic guarantees on real-time delivery," *IEEE Trans. Power Syst.*, vol. 36, no. 4, pp. 2815–2828, 2021.
- [23] H. Cui, F. Li, and K. Tomovic, "Hybrid symbolic-numeric framework for power system modeling and analysis," *IEEE Trans. Power Syst.*, vol. 36, no. 2, pp. 1373–1384, 2021.
- [24] S. Chakrabarti and E. Kyriakides, "Optimal placement of phasor measurement units for power system observability," *IEEE Trans. Power Syst.*, vol. 23, no. 3, pp. 1433–1440, 2008.
- [25] J. Qi, K. Sun, and W. Kang, "Optimal pmu placement for power system dynamic state estimation by using empirical observability gramian," *IEEE Trans. Power Syst.*, vol. 30, no. 4, pp. 2041–2054, 2015.
- [26] M. Picot and F. J. Messina, "Robust autoencoder-based state estimation in power systems," in *2022 IEEE Power & Energy Society Innovative Smart Grid Technologies Conference (ISGT)*, 2022, pp. 1–5.